A Numerical Investigation on Magnetic Pulse Cladding of Bi-Metal Tubes *

Zhisong Fan[1], Haiping Yu[1, 2], Chunfeng Li[1, 2]

[1] School of Materials Science and Engineering, Harbin Institute of Technology, Harbin, China
[2] National Key Laboratory for Precision Hot Processing of Metals, Harbin, China;

Abstract

Bimetal tubes are widely applicable in refrigerating industry, liquid conduit systems and other similar installations. Magnetic pulse cladding (MPC), based on a sequential joining/welding of lapping portions of long tubes, is a novel approach to fabricate bimetal tubes. This work presents an efficient numerical simulation of the MPC process to analyze the dynamic deformation and its effect on cladding result from a numerical view. A 2D axisymmetric model was established and a multi-steps cladding by forming was simulated based on the models similar to an actual MPC process. Between two subsequent steps, the stresses and strains were transferred from previous step to next one. The model predictions and experimental results were compared by the contour of the clad tube and showed an acceptable agreement. The advantages of a new field shaper with tile angle α1 of 3° and angle α2 of 13° were presented, and the magnitude of the magnetic pressure, the stress-strain field and velocity of collision were investigated. The numerical simulation benefits the process knowledge and assists the design of the field shaper.

Keywords

Numerical simulation, Magnetic pulse cladding, Bimetal tube, Field shaper

---

* *This work is based on the results of the National Basic Research Program of China (973 Program) [2011CB012805].*

1 Introduction

Bimetal tubes are widely applicable in refrigerating industry, liquid conduit systems and other similar installations. They have material properties that cannot be obtained from a single material. Enhanced mechanical properties, corrosion resistance, electrical conductivity, and wear resistance are the main industrial demands that can be met in this way [1-2].

Magnetic pulse cladding (MPC), based on a sequential joining/welding of lapping portions of long tubes, is a novel approach to fabricate bimetal tubes. Fig. 1 shows the general outline of MPC derived from the paper of Yu et al. [3].To investigate the dynamic deformation and determine its potential for a certain application, numerical simulation technique is an important part of the research process [4-5].

The general object of this study is to understand the complex phenomenon of deformation and investigate the effect of processing parameters on the quality of a bimetal tube during MPC. The MPC process was simulated by means of ANSYS/LS-DYNA code. The predicted results were validated with the profiles of a deformed tube in experiments.

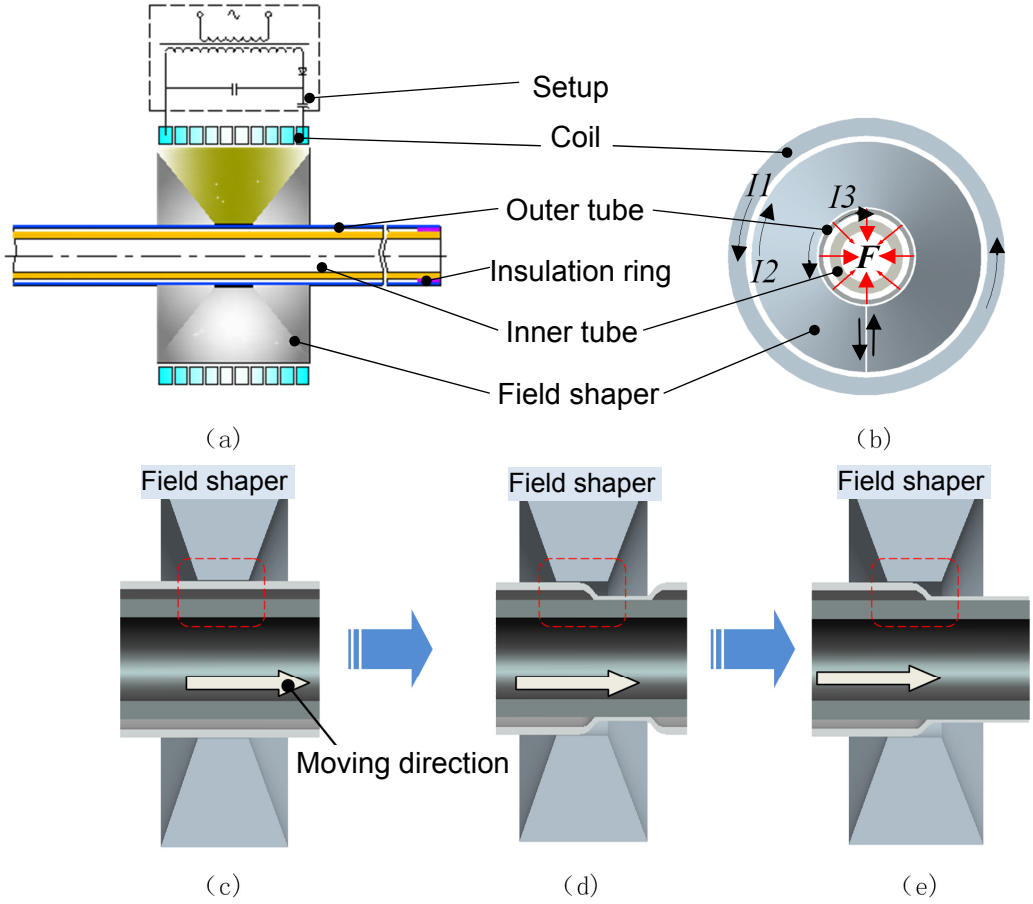

***Figure 1**: Schematic diagram of the MPC process from the published paper of Yu et al. [3]: (a) the setup assembly; (b) the magnetic force exerted on the outer tube; (c) co-axially aligned tubes for the 1st step of the MPC process; (d) the 2nd step of the MPC process with a defined feeding size; (e) the 3rd step of the MPC process with a defined feeding size.*

2 Methodology

2.1 Description of computational model

According to its deformation characteristics, the MPC process can be divided into a series of separate forming sub-steps, namely a “multi-steps” cladding process. Fig. 2 shows the numerical scheme for the proposed “multi-steps” cladding by forming on the basis of ANSYS EMAG/LS-DYNA software platform. In one step of MPC, EM model based on ANSYS/EMAG module was used to calculate the transient magnetic field. Then the resulted equivalent magnetic pressures were acted as the loading condition in mechanical model based on LS-DYNA module to predict the dynamic plastic deformation of the two tubes. When it comes to EM field simulation in the next step of MPC, the coil (including the field shaper) was moved to a new axial position controlled by the feeding size, and the deformed geometry of work piece was input by user-defined subroutines in APDL language. The modified EM model was used to predict the new body forces affected by the new configure of the work piece. For the second and subsequent steps in the mechanical model, the full restart method of the explicit code LS-DYNA was applied to link deformation (such as the stresses and strains) to exhibit a successive deformation sequence.

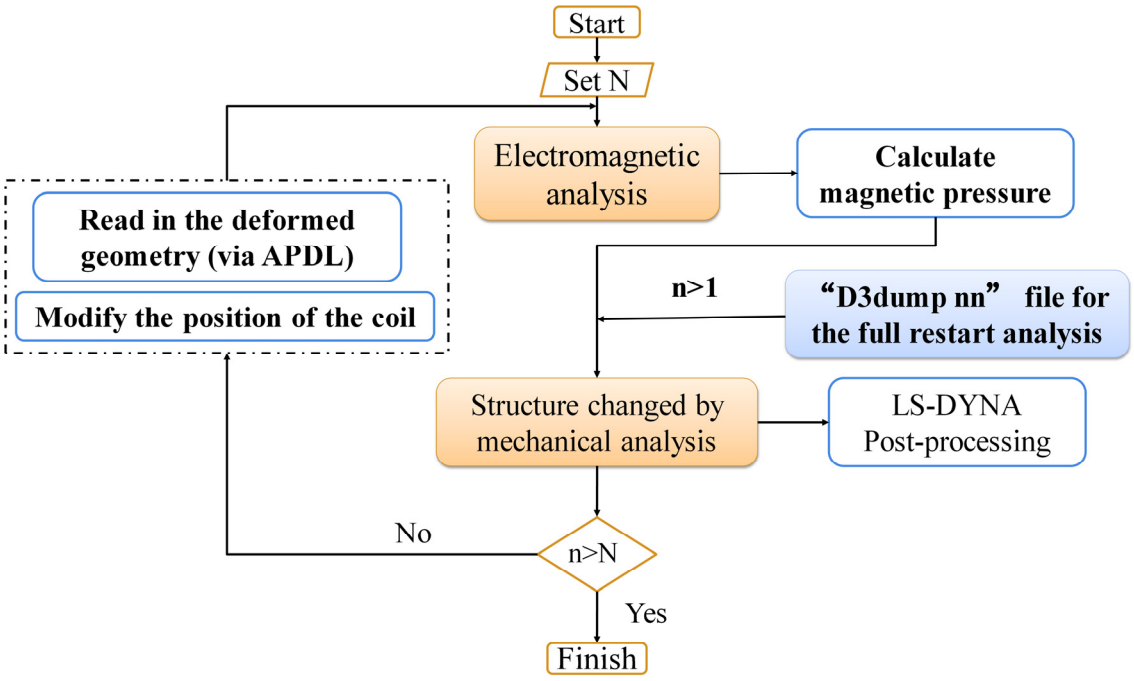

***Figure 2**: Flow chart of simulation procedure for the MPC process using ANSYS/LS-DYNA (N represents the feeding times, n is the ordinal number of N)*

2.2 The FE model and its features

A 2D axisymmetric model as shown in Fig. 3 (a) was established, which makes the most of the experimental geometric symmetry. The EM model of the 1st step of MPC was shown in Fig. 3 (b) and it corresponding mechanical model was shown in Fig. 3 (c).

In the EM simulation phase, the electromagnetic model was excited by a pulse of current through the coil, which is measured experimentally by a Rogowski coil. The typical discharge current is a damped sinusoidal function given as:

$$I = I_0 \exp(-\beta t)\sin(\omega t) \tag{1}$$

where I_0 is the nominal peak value of the discharge current; β is the damping exponent and ω is the angular frequency. The parameters in equation (1) were fitted from the experimentally measured data. The resulted equivalent magnetic pressures were used in this work [6]. The magnetic pressures applied as a loading condition were also via a user subroutine in APDL language.

In the mechanical simulation phase, the strain-rate hardening effect was considered by means of the Cowper-Symonds constitutive model:

$$\sigma = \sigma_y \left[1 + \left(\frac{\dot{\varepsilon}}{C}\right)^P\right] \tag{2}$$

where σ_y is the quasi-static flow stress; $\dot{\varepsilon}$ is the plastic strain rate (s^{-1}); C=6500 s^{-1} and p=0.25 are specific parameters for aluminium and C=40 s^{-1},p=0.2 for steel. The coil and the field shaper were attributed to rigid body. The detailed material parameters were given in Table 1.

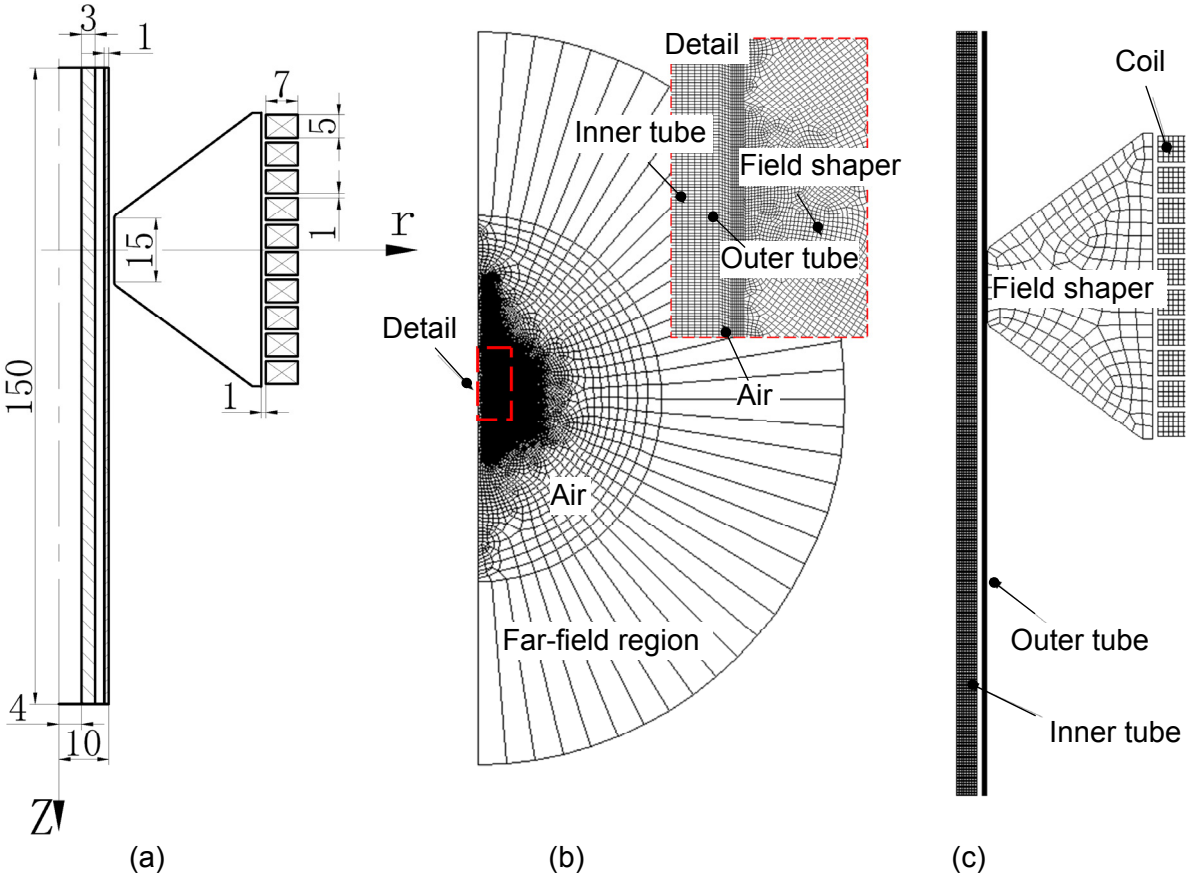

***Figure 3**: Geometry model and finite element region for magnetic pulse cladding system:(a) Geometry model; (b) Electromagnetic field for 1st stage of MPC and detail including tubes and field shaper; (c) Mechanical field of MPC*

Material	Resistivity (Ω•m)	Yield strength σ_s (MPa)	Young's modulus (GPa)
AA3003 (outer tube)	3.4e-8	162	68.6
Mild Steel 1020 (inner tube)	1.0e-7	310	207
Copper (coil and field shaper)	2.17e-8	--	--

Table 1: *Material parameters of the tubes*

2.3 Magnetic pulse cladding experiments

In order to verify simulation results, relevant experiments were carried out. The MPC process was studied experimentally and all basic data could be found in Refs. 3. The verification experiments were performed using 20 kJ EMF systems. The setup has a capacitor with 100 μF capacitance which may be charged to a maximum of 20 kV. The coil has 10-turns with a 5×7 mm cross-section. It was noted that two kinds of field shaper were modelled in this work for the reason that it could be of much value in designing its geometry. Geometry parameters of two kinds of field shapers were derived from Ref. 3, as shown in Fig. 4.

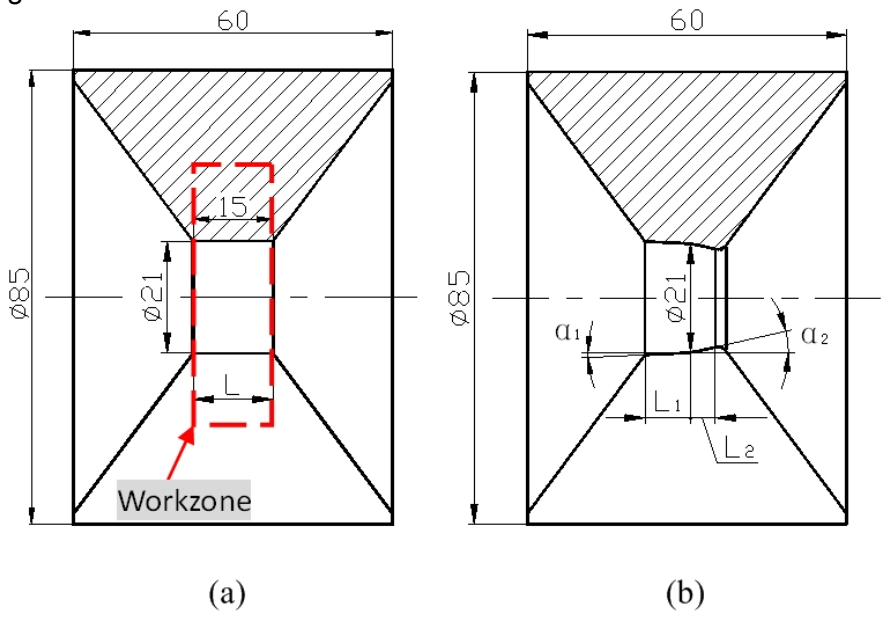

Figure 4*: The cross-section of two kinds of field shaper geometry: (a) the constant cross-section field shaper (C-field shaper) and (b) the profiled field shaper (P-field shaper)*

3 Results and discussion

3.1 Verification experiments

Fig. 5 (a) shows the final formed part with the predicted radial displacement. To extend the 2D model into a 3D format is to compare it with the experimental sample formed by MPC using the C-field shaper. The ripple defect could be observed in the outer surface of the clad tube in Fig. 5 (b). The height of the ripple was measured via the distribution of the final radial displacement, as illustrated in Fig. 6. Fig. 7 presented an optical micrograph image of the transition region including one ripple. The height of a hump (about 0.06 mm) is slightly smaller than the predicted height (0.09 mm).

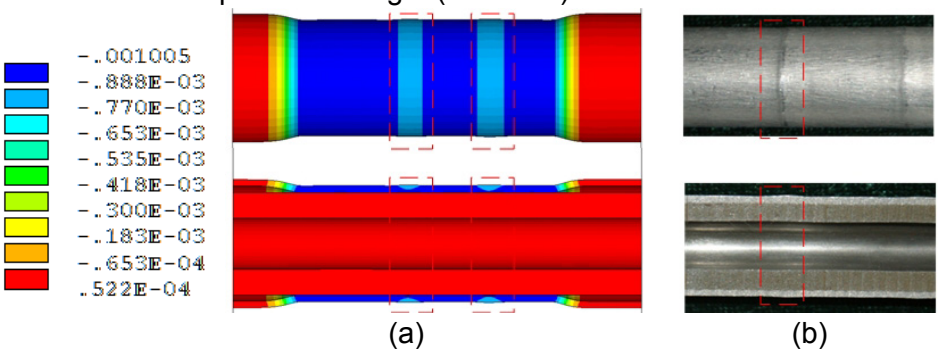

***Figure 5**: Predicted and experimental profiles deformed by MPC: (a) Predictions of final radial displacement contours and (b) the ripple in the surface of the formed part*

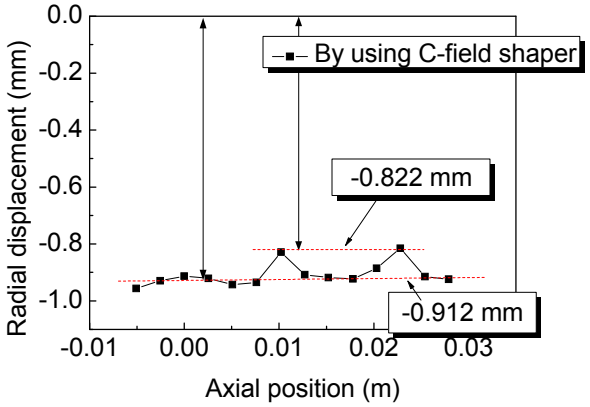

***Figure 6**:The distribution of the final radial displacement of the outer tube for three steps of MPC*

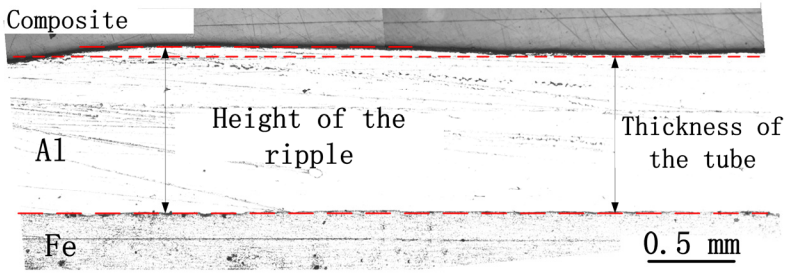

***Figure 7**: Cross-section for one ripple in the optical micrograph image*

3.2 Deformation behaviours in local transition region

3.2.1 The case of C-field shaper

As stated earlier, the magnetic pulse cladding process consists of a repeated unit. Fig. 8 showed the characteristics of the magnetic field in the second step by using C-field shaper. The magnetic lines diffuse through the transition zone. And the induced current in the transition zone is smaller than that flowing in its adjacent region. The resulting magnetic pressure was illustrated in Fig. 9. So the ripple defect generates in the transition zone.

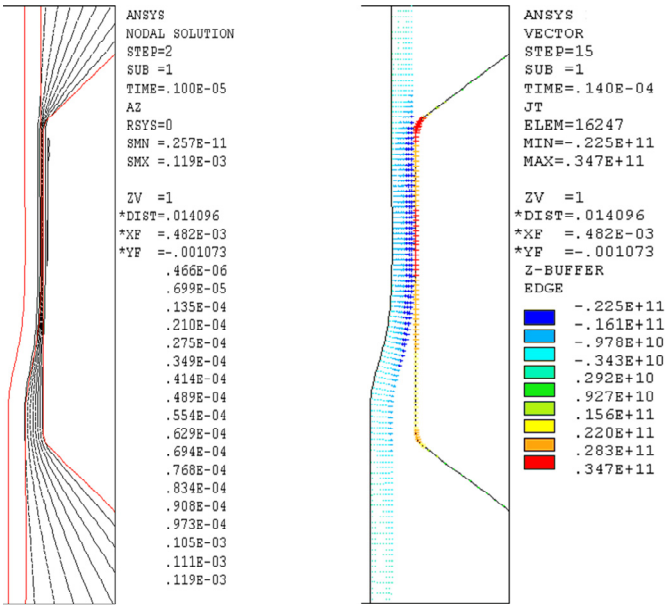

(a) (b)

***Figure 8**: Characteristics of the magnetic field in the early time of the 2nd step of MPC: (a) Distributions of magnetic flux line; (b) Contours of induced current on the workpiece and the C-field shaper*

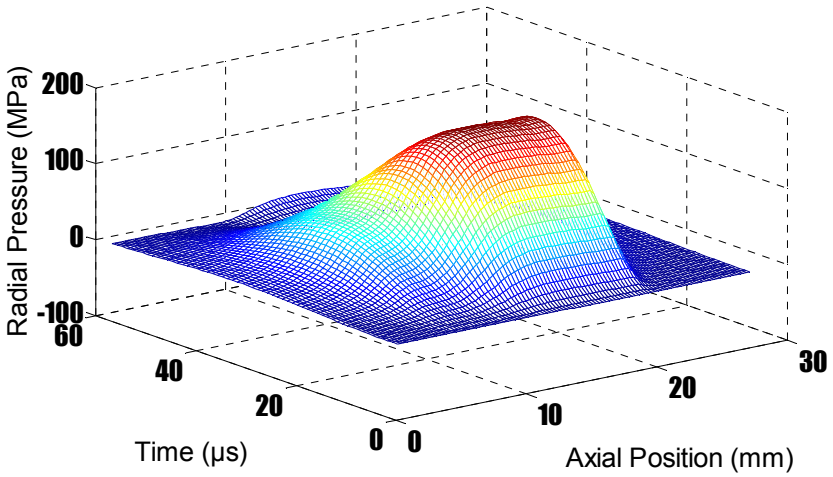

***Figure 9**: The distribution of magnetic pressure over time along the axial direction during the 2nd step of MPC in the case of C-field shaper*

3.2.2 Modelling of the P-field shaper

The transition geometry between two cladding steps depends on magnetic pressures distribution and the latter lies on the relative position between outer tube and working zone of field shaper. The smaller gap between them causes larger pressure acting on the outer tube. Therefore, to fit the profile of the transition geometry, the profile of working zone of field shaper was changed and a P-field shaper was proposed. The P-field shaper with a tile angle α1 of 3° and angle α2 of 13° was modelled. Fig. 10(a) shows the magnetic flux lines in the second step of MPC. In the early time, all the magnetic flux lines are restrained in the gap between the outer tube and the P-field shaper. Due to the tile angle of 13°, the density of the magnetic flux line in transition zone increases compared to that of the C-field shaper used. Fig. 10(b) and (c) presented the distribution of the induced current and Lorentz's force. Fig. 11 showed the resulting distribution of magnetic pressure. The peak locating in the transition zone is about 200 MPa, 2.5 times of that of the C-filed shaper in same region shown in Fig. 9. Away from the transition zone, the magnetic pressure decreases slightly due to the setting of title angle α1 of 3°. This kind of distribution characteristic of magnetic forces helps to deform the transition zone and obtain the oblique collision during the multi-step stage of MPC.

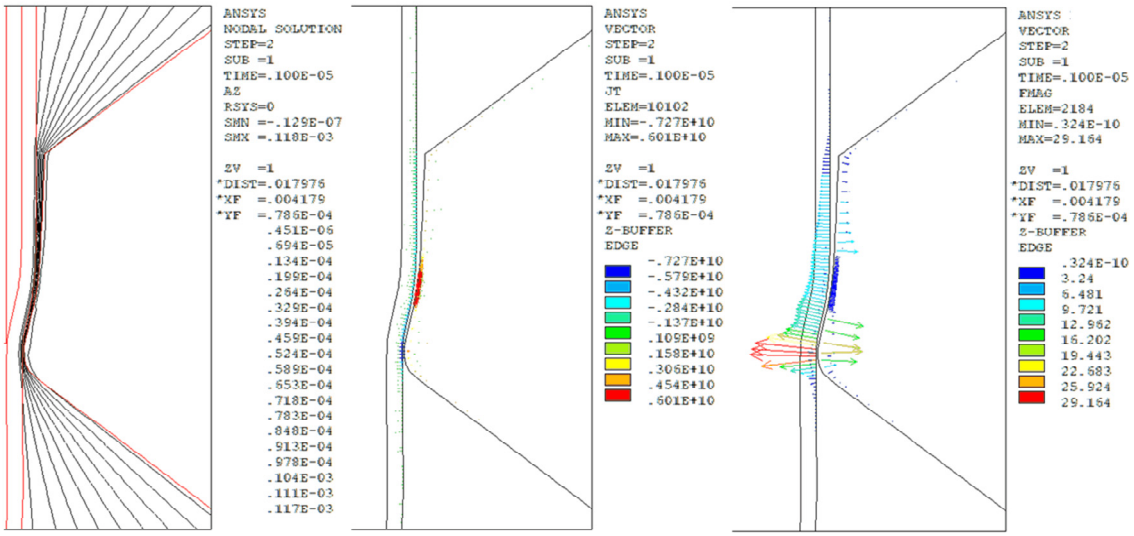

(a) (b) (c)

***Figure 10**: characteristics of the magnetic field in the early time of the 2nd step of MPC: (a) Distributions of magnetic flux line; (b) Contours of induced current on the work piece and the P-field shaper; (c) The distribution of the vector resultant of the Lorentz's forces developed in the work piece and the P-field shaper.*

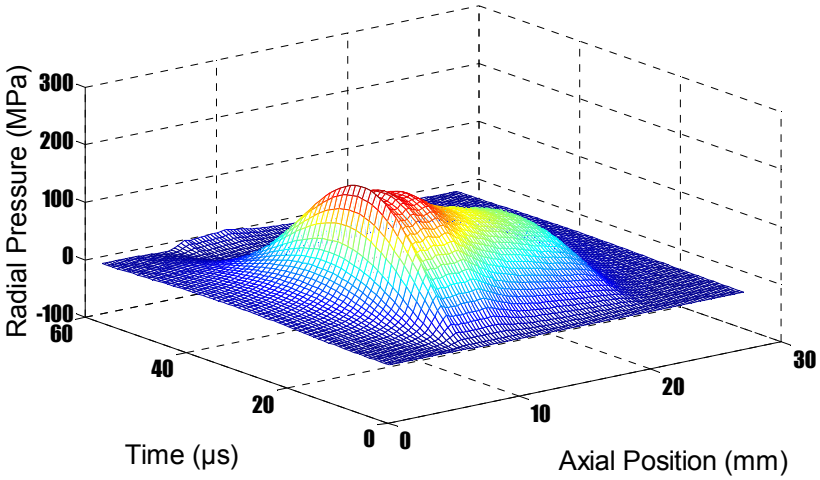

***Figure 11**: The distribution of magnetic pressure over time along the axial direction during the 2nd step of MPC.*

3.2.3 Comparison of two collision mode

Fig. 12 showed the comparison of clad tubes' geometry with the original and the improved field shaper. Fig. 13 presented the results of the bonding area, conducted by the peeling test. As can be seen, the bonding area concentrated in the first collision region and the bonding area was about 22% of the whole cladding area in the C-field case. By using the P-field shaper, the bonding area increased to 47%, as shown in Fig. 13. With improved field shaper, the clad tube deforms in a desired manner that it can dynamically impact the base one obliquely in a cladding step. The numerical simulation could assist the design of the field shaper.

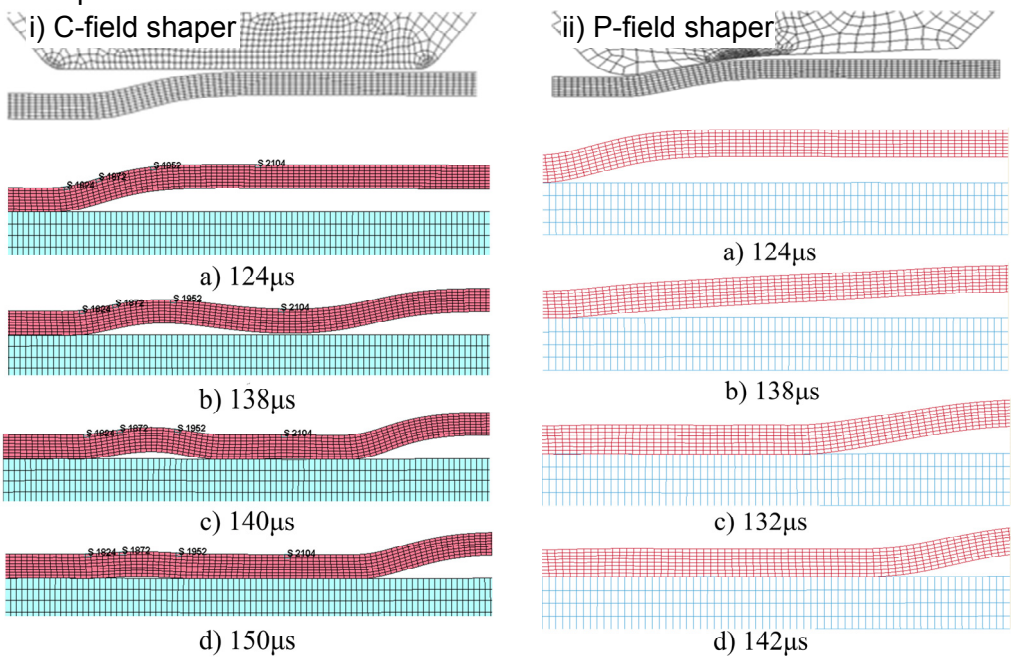

***Figure 12**: LS-DYNA prediction of the change of geometry of the clad tube during the second step of MPC: (i) in the case of C-field shaper and (ii) in the case of P-field shaper*

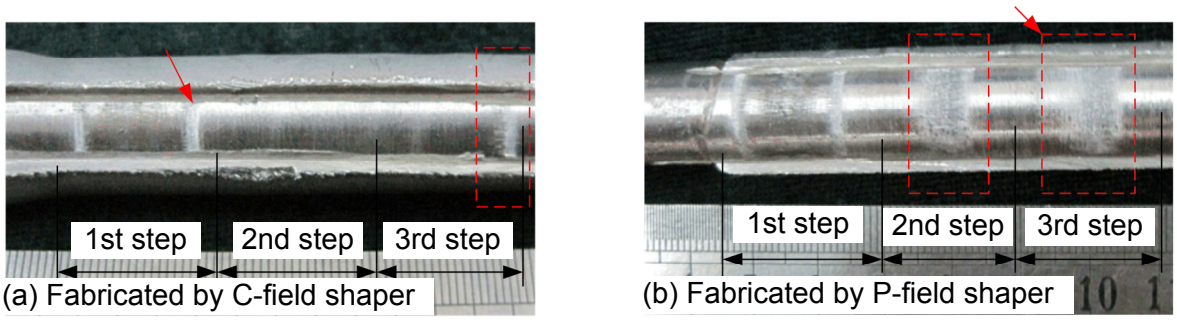

***Figure 13**: Comparison of the rate of the bonding area: (a) in the case of C-field shaper and (b) in the case of P-field shaper*

4 Conclusions

In the present paper, the basic aspects of the magnetic pulse cladding process were numerically simulated. The proposed numerical method was validated by the results of contour of the deformed tube in experiments. The following conclusions are drawn:

1) Based on the models similar to an actual MPC process, a numerical scheme for multi-steps cladding by forming was proposed. The scheme was successfully applied to simulate the MPC process that provides the basis for further investigating the deformation mechanism of MPC.

2) In the subsequent cladding phase, the inharmonious deformation results in the ripple defect in the surface of the clad tube. The profile of working zone of field shaper can be changed to fit the profile of the transition geometry to shape the distribution of the magnetic field.

3) The P-field shaper improves the distribution of the magnetic pressure during the multi-step stage of MPC. With improved field shaper, the outer tube deforms in a desired manner that it can dynamically impact the base one obliquely in a cladding step.

References

[1] Schulz, W.; Worringer, J.; Osborn, D.: Process for the manufacture of cladded metal pipes. United States Patent, No. 5940951, 1999.

[2] Mohebbi, M. S.; Akbarzadeh, A.: Fabrication of copper/aluminum composite tubes by spin-bonding process: experiments and modeling. The International Journal of Advanced Manufacturing Technology, 54(9-12), p. 1043-1055, 2011.

[3] Yu H. P.; Fan Z. S.; Li C. F,: Magnetic pulse cladding of aluminum alloy on mild steel tube [J]. Journal of Materials Processing Technology, 214(2): p. 141-150, 2014.

[4] Oliveira, D. A.; Worswick, M. J.; Finn, M.; Newman, D.: Electromagnetic forming of aluminum alloy sheet: free-form and cavity fill experiments and model. Journal of Materials Processing Technology, 170(1), p. 350-362, 2005.

[5] Fenton, G. K.; Daehn, G. S.: Modeling of electromagnetically formed sheet metal. Journal of Materials Processing Technology, *75*(1), p. 6-16, 1998.

[6] Psyk, V.; Risch, D.; Kinsey, B.L.; Tekkaya, A.E.; Kleiner, M.: Electromagnetic forming-A review. Journal of Materials Processing Technology 211, 787-829, 2011.